

Flutter-Prediction Tool for Flight-Test-Based Aeroelastic Parameter-Varying Models

Dario H. Baldelli* and Jie Zeng†

ZONA Technology Inc., Scottsdale, Arizona 85258

Rick Lind‡

University of Florida, Gainesville, Florida 32611

and

Chuck Harris§

U.S. Air Force Flight Test Center, Edwards Air Force Base, California 93253

DOI: 10.2514/1.36584

In this work, a parameter-varying estimation framework is proposed to increase the efficiency of flight testing. The framework generates a set of tools to rapidly evaluate parameters required to certify an aircraft during envelope expansion. The primary innovation is a generalized aeroelastic parameter-varying framework that allows for a variety of approaches and test procedures. The framework considers the variations of aircraft parameters due to flight conditions. The core algorithms are based on the well-developed linear fractional transformation algebra and μ analysis for aeroelastic/aeroservoelastic systems. They are built upon an integrated parameter-estimation framework that is robust enough to tolerate real-world flight-testing environments. Two application cases were successfully solved using the algorithms developed during this work. The first case study involved a generic pitch and plunge linear aeroelastic wind-tunnel model. In the second case study, flight-test data from the Aerostructure Test Wing program were used to demonstrate the feasible application of the core algorithms using data coming from actual flight-test programs.

Nomenclature

$A(\omega)$	= denominator matrix polynomial
A_k	= nonzero matrix coefficients in $A(\omega)$
A^i, B^i, C^i, D^i	= state-space quadruple matrices related to \bar{P}_i
$B(\omega)$	= numerator matrix polynomial
B_{ik}	= nonzero matrix coefficients in $B(\omega)$
$B^i(q)$	= a priori orthonormal basis function at the i th waypoint
f_{m0}, f_{m1}, f_{m2}	= coefficients in the flutter margin equation
$P(\omega)$	= complex frequency response function
\bar{P}_i	= estimated linear time-invariant system at the i th waypoint
q	= forward shift operator
q^i	= dynamic pressure at the i th waypoint
U	= airspeed
\bar{u}	= noisy aeroelastic model input signal
w	= input from uncertain dynamic-pressure parameter
\bar{y}	= noisy aeroelastic model output signal
z	= output to uncertain dynamic-pressure parameter
$\gamma(\cdot)$	= nonlinear operator matrix
δ_q^i	= perturbation to dynamic pressure at the i th waypoint

θ	= vector of unknown parameters
μ	= structural singular value
ω	= frequency of oscillation

Introduction

FLIGHT flutter programs are devised to verify whether the aircraft is aeroelastically stable within its operational flight envelope. They are among the most expensive part of the aircraft certification process; in addition, they can tie up an aircraft for several months while the flutter flights are being performed. Hence, any reduction in the number of flights required to clear an aircraft from flutter will be beneficial to the aerospace industry.

Flutter and flying-quality testing, which must be done for new and modified aircraft, incurs dramatic time and cost because of the dangers associated with encountering unpredicted instabilities. The common approach for envelope expansion is to take the aircraft to a stabilized test point and measure data primitives (i.e., vibration data). Data from the test points are analyzed to predict the speed at which flutter may be encountered. The envelope is expanded by increasing the airspeed at successive test points until the data analysis indicates that the airspeed is nearing the flutter speed.

Several methods are traditionally used for the data analysis and prediction of the flutter speed. The most common method is to analyze damping levels that vary with flight condition and extrapolate the resulting trends [1]. Another common method is to use the concept of a flutter margin in conjunction with a formulation to predict the onset of flutter [2]. Validated wind-tunnel flutter-model prediction algorithms used for both open- and closed-loop flutter-suppression systems are also available [3,4]. More recently, a wing-model testbed was used at NASA Dryden Flight Research Center to evaluate several of these methods to predict the onset of flutter [5]. Each of these methods have been proven useful for flight-test programs; however, their predictions are never accepted with complete confidence. Damping certainly will decrease to zero as the aircraft approaches flutter, but the nonlinear variation of damping with airspeed may make accurate extrapolation difficult. Similarly, the flutter margin is technically correct for low-order flutter, but it will predict the correct speed only if the flutter mechanism is actually

Presented as Paper 6301 at the AIAA Atmospheric Flight Mechanics Conference and Exhibit, Hilton Head South Carolina, 20–23 August 2007; received 11 January 2008; revision received 17 July 2008; accepted for publication 18 July 2008. Copyright © 2008 by Dario H. Baldelli. Published by the American Institute of Aeronautics and Astronautics, Inc., with permission. Copies of this paper may be made for personal or internal use, on condition that the copier pay the \$10.00 per-copy fee to the Copyright Clearance Center, Inc., 222 Rosewood Drive, Danvers, MA 01923; include the code 0731-5090/09 \$10.00 in correspondence with the CCC.

*Aeroservoelasticity and Control Manager; currently Associate Technical Fellow, Northrop Grumman Corporation, Vehicle Management System, Guidance, Navigation, and Control. Senior Member AIAA.

†Research and Development Control Engineer.

‡Assistant Professor. Senior Member AIAA.

§Aerospace Engineer, 412th Test Wing. Member AIAA.

low-order and accurate dampings are computed for the necessary modes. Thus, these methods are valuable but must be applied with caution.

A variety of difficulties arise in the flight-testing process. Most notably, the data from which the dynamics must be determined are often quite poor from an information-theoretical viewpoint. These data are corrupted with significant levels of noise that may completely obscure any observations of the dynamics. The excitation used to generate the data is often inexact and unknown and fails to provide injected energy at all frequencies. Furthermore, the aircraft needs to limit the time spent during testing, and so data sets are necessarily short. These difficulties combine to present a harsh environment for data analysis.

In this work, a data-based parameter-varying model framework is sought to rapidly evaluate and accurately predict parameters that are required to certify an aircraft during flutter envelope-expansion programs. The fundamental concept seeks to evaluate the influence of flight condition on dynamics. The proposed framework calls for parameter-varying models to be quickly tuned with modal information embedded in the flight-test data.

Development of Parameter-Varying Models

The core algorithms are built upon an integrated parameter-estimation framework that proved to be robust enough to tolerate real-world flight-testing environments. They are based on the well-developed linear fractional transformation (LFT) algebra and μ analysis for aeroelastic/aeroservoelastic systems [6–8]. The procedure calls for parameter-varying models to be quickly tuned with modal information embedded in the flight-test data, and linear/nonlinear models can be used to highlight the actual dynamics embedded in the flight-test data.

The concept, as shown in Fig. 1, has data from across the flight envelope being filtered to extract data primitives which are fitted through a regression to derive parameter-varying estimates. The framework adopts the methodology of aeroelastic parameter-varying (APV) models. They are based on a technique to model uncertain nonlinear systems for which the dynamics can be a function of the system configuration and operating conditions [9,10]. The advantage

of using the APV models is that the underlying dynamics can further be extended as a function of the flight condition.

The APV model performs this estimation through a four-step process that uses a unifying framework to represent the resulting parameters. These steps are defined as follows:

- 1) Flight-test data-gathering (Fig. 1, block 1).
- 2) Filtering techniques using short- and long-duration data segments (Fig. 1, block 2).
- 3) Parameter-varying model development (Fig. 1, block 3).
- 4) Flutter-predictor development (Fig. 1, block 4).

Hence, this framework develops parameter estimation for the parameter-varying aircraft dynamics. The filtering process and subsequent regression considers the variation of the parameters as constrained by the underlying variation across flight conditions. In this way, the process maximizes the use of present and past information to obtain optimal estimates of parameters that are more accurate than simply filtering a small set of data. The inclusion of variation with the flight condition is a powerful addition that dramatically increases the information, along with providing an underlying structure, available to the estimation problem.

Flight-Test Data-Gathering

The process of envelope expansion would be greatly facilitated if the onset of instabilities could be predicted using a minimum amount of data. As such, the purpose of data-gathering is to properly perform informative experiments, as well as to record the aircraft inputs and outputs. Estimation of data primitives is carried out primarily from the dynamic response of the aircraft to specific control inputs. Short-duration data segments ($t \leq 5$ s) recorded using multistep input signals and/or long-duration data segments ($t \leq 35$ s) composed by frequency sweeps are traditionally used for aircraft system-identification purposes. The former will require some a priori knowledge of the dominant frequency of the aircraft under analysis, whereas the latter does not have that constraint.

Evaluating the techniques for flying-quality and instability prediction in the context of using flight data is quite useful for determining the properties needed by the parameter-varying estimation (PVE) framework.

Filtering Techniques: Modal Parameter Estimation

The frequency-domain PolyMAX filtering technique is proposed to extract modal parameter information from short- and long-duration flight-test data segments [11]. Consider a set of noisy complex frequency response function (FRF) measurement data $G(\omega_j)$ ($j = 1, \dots, N$). The approximation of the data by a model $P(\omega_j)$ is addressed by considering the following additive error:

$$E(\omega_j) = G(\omega_j) - P(\omega_j), \quad j = 1, \dots, N \quad (1)$$

Then it is assumed that the model $P(\omega)$ can be represented by a right polynomial fraction matrix given by

$$P(\omega) = [B(\omega)][A(\omega)]^{-1} \quad (2)$$

where $P(\omega) \in \mathcal{C}^{p \times m}$ is the FRF matrix with p outputs and m inputs, $B(\omega) \in \mathcal{R}^{p \times m}$ is the numerator matrix polynomial, and $A(\omega) \in \mathcal{R}^{m \times m}$ is the denominator matrix polynomial.

For a model with m inputs and p outputs, each row of the right matrix fraction model can be written as follows:

$$P_i(\omega) = [B_i(\omega)][A(\omega)]^{-1}, \quad i = 1, 2, \dots, p \quad (3)$$

where the polynomial matrix $B_i(\omega)$ is parameterized by

$$B_i(\omega) = \sum_{k=0}^{n_b} B_{ik} \xi_k(\omega) \quad (4)$$

where $B_{ik} \in \mathcal{R}^{1 \times m}$, and n_b are the number of nonzero matrix coefficients in $B(\omega)$, or the order of $B(\omega)$, and $\xi_k(\omega)$ are the polynomial basis functions. Note that for continuous-time models, $\xi_k(\omega) = -i\omega_k$, and for discrete-time models, $\xi_k(\omega) = e^{-i\omega_k T}$ (where

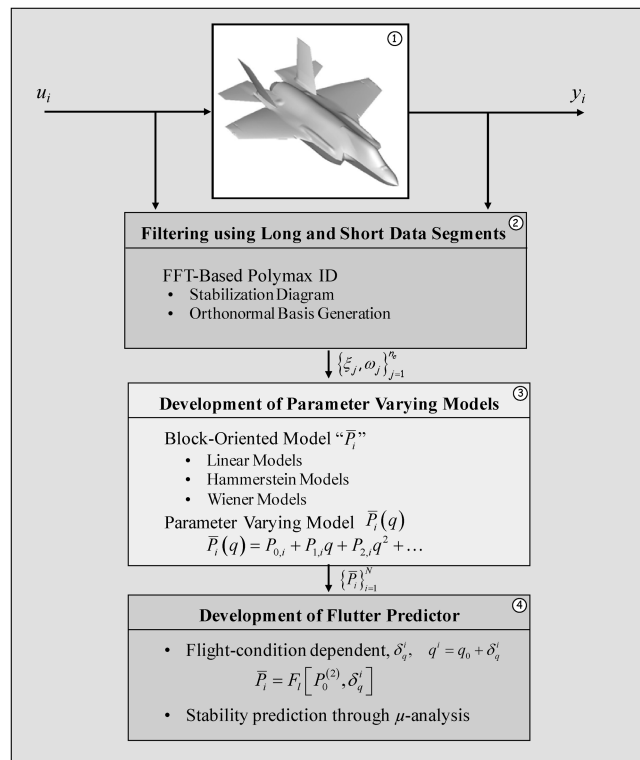


Fig. 1 Aeroelastic parameter-varying estimation framework.

T is the sampling time). In what follows, only the discrete-time case will be considered.

The polynomial matrix $A(\omega)$ is parameterized by

$$A(\omega) = \sum_{k=0}^{n_a} A_k \xi_k(\omega) \quad (5)$$

where $A(\omega) \in \mathcal{R}^{m \times m}$, and n_a are the number of nonzero matrix coefficients in $A(\omega)$.

Defining

$$\beta_i = [B_{i0}, B_{i1}, \dots, B_{in_b}] \in \mathcal{R}^{(n_b+1) \times m}, \quad i = 1, 2, \dots, p$$

The polynomial matrix coefficients $\beta_i \in \mathcal{R}^{(n_b+1) \times m}$ and $A_k \in \mathcal{R}^{m \times m}$ are stacked in the following way for computational purposes:

$$\theta = [\beta_1, \dots, \beta_p, A_0, \dots, A_{n_a}] \quad (6)$$

where the parameter θ is the unknown coefficient that needs to be estimated. Based on the framework of the least-squares approach, the linear least-squares equation error is obtained by right multiplying $A(\omega)$ in Eq. (3), which yields

$$\varepsilon_i(\omega) = W_i(\omega)[B_i(\omega) - G_i(\omega)A(\omega)] \quad (7)$$

where W_i is a scalar weighting function for each output. The parameter θ is calculated by minimizing the cost function $V(\theta)$:

$$\hat{\theta} = \min_{\theta}(V(\theta)) = \min_{\theta} \sum_{i=1}^p \sum_{k=1}^N \text{tr}\{\varepsilon_i(\omega_k, \theta)^H \varepsilon_i(\omega_k, \theta)\} \quad (8)$$

In general, a constraint $A_0 = I_m$ is set to obtain a stable model to fit the measured frequency-domain data. Here, a constraint $A_{n_a} = I_m$ is adopted to extract physical modes from the measured frequency-domain data [11]. With $A_{n_a} = I_m$, the poles of the estimated model are separated into stable physical poles and unstable mathematical poles, from which a clean stabilization diagram can be obtained, and the physical modal parameters of the real system can be estimated from a quick evaluation of the generated stabilization diagram [12].

The stabilization diagram assumes an increasing model order (number of poles noted in the ordinate axis), and it indicates where the poles are located on the frequency axis. As a rule, positive damping poles are not considered in the plot. Physical poles will appear as stable poles, independent of the number of the assumed model order. On the other hand, *mathematical* poles that intend to model the noise embedded in the data will change with the assumed model order.

Generation of Aeroelastic Parameter-Varying Models

At each waypoint, some kind of *mapping* between the input and output of the linear or nonlinear aeroelastic needs to be performed. Hence, in this work the mapping was represented using block-oriented models that consist of the interconnection of a linear time-invariant (LTI) operator \bar{P}_i and a memoryless nonlinearity $\gamma_i(\cdot)$, where $\gamma_i(\cdot) = 1$ if the estimated model is linear.

Figures 2a and 2b schematically depict the Hammerstein and Weiner block-oriented models, respectively. The underlying structure of a generic block-oriented model assumes that the steady-state behavior is determined by the static nonlinearity, and the dynamic behavior is determined altogether by the static map and the LTI part. Note that the block-oriented method allows that any a priori knowledge about the dynamics of the flexible structure can be included as an affine parametric component of the identified system, expressed in terms of a suitable selection of the poles of the basis function set. It also represents a low-cost and noniterative solution in terms of identification computations [8].

Hence, at the i th waypoint, the model will consist of a linear or nonlinear operator $\gamma_i(\cdot)$ in series connection with a LTI system described by its transfer function matrix:

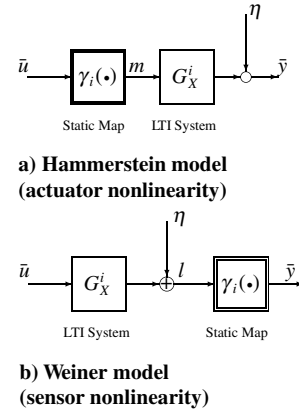


Fig. 2 Block-oriented nonlinear models.

$$\bar{P}_i(q) = \sum_{l=0}^{p-1} b_l B_l^i(q) \quad (9)$$

where $\{B^i(q)\}_{l=0}^{p-1}$ is the a priori set of orthonormal basis tuned with underlying modal dynamics embedded in the aeroelastic waypoint data and q is the forward shift operator. The required modal parameters are a set composed by the natural frequencies ω_k and damping ratios ζ_k (i.e., $\{\omega_k, \zeta_k\}_{k=1}^{N_p} = 1$, where N_p is the number of single modes accurately estimated by the PolyMAX method and the stabilization diagram of step 2 in Fig. 1). For linear/nonlinear identification of mechanical flexible systems, it is suggested to employ the two-parameter Kautz filters to generate a network of cascaded all-pass filters. Then a matrix factorization technique, based on its state-space realization, is used to construct the set of orthonormal basis functions $\{B^i(q)\}_{l=0}^{p-1}$ [13].

In addition, the dynamic-pressure dependency is included by fitting the state-space model of the identified linear system $\bar{P}_i(A^i, B^i, C^i, D^i)$ ($i = q_0 \in [q_{\text{lower}}, \dots, q_{\text{upper}}]$) to a polynomial function of the dynamic pressure. In this simple way, the proposed flutter-prediction framework is devised to predict the measured responses from the current dynamic pressure during the flight-test program. Specifically, using a quadratic matrix polynomial function of the dynamic pressure, that is [9,10],

$$\begin{Bmatrix} \dot{x} \\ \ddot{y}^i \end{Bmatrix} = \underbrace{\begin{bmatrix} A^i & B^i \\ C^i & D^i \end{bmatrix}}_{\bar{P}_i} \begin{Bmatrix} x \\ \ddot{u}^i \end{Bmatrix} \quad (10)$$

$$= \begin{bmatrix} A_0 + A_1 q^i + A_2 (q^i)^2 & B_0 + B_1 q^i + B_2 (q^i)^2 \\ C_0 + C_1 q^i + C_2 (q^i)^2 & D_0 + D_1 q^i + D_2 (q^i)^2 \end{bmatrix} \begin{Bmatrix} x \\ \ddot{u}^i \end{Bmatrix} \quad (11)$$

Equation (11) results in a form that can easily be parameterized around the dynamic-pressure perturbation parameter δ_q^i , such that

$$q^i = q_0 + \delta_q^i \quad (12)$$

where q_0 is the i th waypoint's dynamic-pressure value. By replacing Eq. (12) into Eq. (11), the state and output equations are expressed as follows:

$$\begin{aligned} \dot{x} &= [A_0 + A_1(q_0 + \delta_q^i) + A_2(q_0 + \delta_q^i)^2]x \\ &\quad + [B_0 + B_1(q_0 + \delta_q^i) + B_2(q_0 + \delta_q^i)^2]\ddot{u}^i \\ &= [A_0 + A_1q_0 + A_2q_0^2]x + [B_0 + B_1q_0 + B_2q_0^2]\ddot{u}^i \\ &\quad + [(A_1 + 2q_0A_2)x + (B_1 + 2q_0B_2)\ddot{u}^i]\delta_q^i + [(A_2x + B_2\ddot{u}^i)\delta_q^i]\delta_q^i \end{aligned}$$

$$\begin{aligned} \ddot{y}^i &= [C_0 + C_1q_0 + C_2q_0^2]x + [D_0 + D_1q_0 + D_2q_0^2]\ddot{u}^i \\ &\quad + [(C_1 + 2q_0C_2)x + (D_1 + 2q_0D_2)\ddot{u}^i]\delta_q^i \\ &\quad + [(C_2x + D_2\ddot{u}^i)\delta_q^i]\delta_q^i \end{aligned}$$

Using new fictitious feedback signals z_j and w_j ($j = 1, \dots, 6$) defined by the next set of equations,

$$\begin{aligned} z_1 &= (A_1 + 2q_0 A_2)x + (B_1 + 2q_0 B_2)\bar{u}^i, & w_1 &= \delta_q^i z_1 \\ z_2 &= A_2 x + B_2 \bar{u}^i, & w_2 &= \delta_q^i z_2 & z_3 &= w_2, & w_3 &= \delta_q^i z_3 \\ z_4 &= (C_1 + 2q_0 C_2)x + (D_1 + 2q_0 D_2)\bar{u}^i, & w_4 &= \delta_q^i z_4 \\ z_5 &= C_2 x + D_2 \bar{u}^i, & w_5 &= \delta_q^i z_5, & z_6 &= w_5, & w_6 &= \delta_q^i z_6 \end{aligned} \quad (13)$$

Eq. (10) can now be defined as a function of the state x , the input \bar{u}^i , and the perturbation signals w_j ($j = 1, \dots, 6$):

$$\dot{x} = [A_0 + A_1 q_0 + A_2 q_0^2]x + [B_0 + B_1 q_0 + B_2 q_0^2]\bar{u}^i + w_1 + w_3 \quad (14)$$

$$\bar{y}^i = [C_0 + C_1 q_0 + C_2 q_0^2]x + [D_0 + D_1 q_0 + D_2 q_0^2]\bar{u}^i + w_4 + w_6 \quad (15)$$

Clearly, this transformation allows the operator \bar{P}^i to be sought as a parameter-varying (PV) system expressed as a lower LFT system. Figure 3 schematically depicts the devised dynamic-pressure-dependent APV model:

$$\begin{Bmatrix} \bar{y}^i \\ z \end{Bmatrix} = F_l[\bar{P}^{(2)}(q_0), \delta_q^i] \begin{Bmatrix} \bar{u}^i \\ w \end{Bmatrix} \quad (16)$$

where the signals z and w are defined as follows:

$$\begin{aligned} z &\triangleq [z_1^T \ z_2^T \ z_3^T \ z_4^T \ z_5^T \ z_6^T]^T \\ w &\triangleq [w_1^T \ w_2^T \ w_3^T \ w_4^T \ w_5^T \ w_6^T]^T \end{aligned}$$

The resulting time-invariant linear operator $\bar{P}^{(2)}(q_0)$ is a function of the nominal waypoint dynamic pressure q_0 and is defined as follows:

$$\begin{aligned} \bar{P}^{(2)}(q_0) &= \\ &= \begin{bmatrix} A_0 + A_1 q_0 + A_2 q_0^2 & B_0 + B_1 q_0 + B_2 q_0^2 & I & 0 & I & 0 & 0 & 0 \\ C_0 + C_1 q_0 + C_2 q_0^2 & D_0 + D_1 q_0 + D_2 q_0^2 & 0 & 0 & 0 & I & 0 & I \\ A_1 + 2q_0 A_2 & B_1 + 2q_0 B_2 & 0 & 0 & 0 & 0 & 0 & 0 \\ A_2 & B_2 & 0 & 0 & 0 & 0 & 0 & 0 \\ 0 & 0 & 0 & I & 0 & 0 & 0 & 0 \\ C_1 + 1q_0 C_2 & D_1 + 2q_0 D_2 & 0 & 0 & 0 & 0 & 0 & 0 \\ C_2 & D_2 & 0 & 0 & 0 & 0 & 0 & 0 \\ 0 & 0 & 0 & 0 & 0 & 0 & I & 0 \end{bmatrix} \end{aligned} \quad (17)$$

The operator $\bar{P}^i = F_l[\bar{P}^{(2)}(q_0), \delta_q^i]$ is now computed as a feedback arrangement that explicitly considers dependency on flight conditions. This parameter-varying model is sought to predict the dynamic behavior of the aeroelastic system at a higher dynamic pressure starting from the waypoint's nominal dynamic-pressure value q_0 . At each dynamic pressure, a parameter-varying model is computed based on a least-squares fit of the identified model \bar{P}^i , considering data recorded up to the actual waypoint's dynamic-pressure value.

Note that the linear operator \bar{P}^i in Eq. (10) can also be represented using a cubic matrix polynomial function of the dynamic pressure:

$$\begin{aligned} \bar{P}_i &= \\ &\equiv \left[\frac{A_0 + A_1 q^i + A_2 (q^i)^2 + A_3 (q^i)^3 B_0 + B_1 q^i + B_2 (q^i)^2 + B_3 (q^i)^3}{C_0 + C_1 q^i + C_2 (q^i)^2 + C_3 (q^i)^3 D_0 + D_1 q^i + D_2 (q^i)^2 + D_3 (q^i)^3} \right] \end{aligned} \quad (18)$$

Hence, a third-order flutter predictor can be defined as follows:

$$\bar{P}_i = F_l[\bar{P}^{(3)}(q_0), \delta_q^i] \quad (19)$$

where the operator $\bar{P}^{(3)}(q_0)$ is a cubic function of the nominal dynamic pressure q_0 and is constructed in a similar manner to that previously described for $\bar{P}^{(2)}(q_0)$.

In both cases, quadratic or cubic, the polynomial matrices can actually be computed in an online fashion such that the parameter dependency is updated after each waypoint to get variations that are optimal in a least-squares sense. Note that the resulting model is consistently formulated within the μ analysis to predict the flutter-instability boundary *online*.

Clearly, the inclusion of parameter dependency simplifies the task of predicting the onset of aeroelastic and/or aeroservoelastic instabilities. The analysis simply needs to iterate over the dynamic pressure by considering the model \bar{P}^i , which is already parameterized around the dynamic pressure.

Development of Flutter Prediction for Data-Based APV Models

Figure 3 schematically depicts the dynamic-pressure-dependent APV model generated by including the dynamic-pressure perturbation parameter δ_q^i . Therefore, the necessary condition for the existence of flutter is stated in the following Lemma [14].

Lemma: Given the plant \bar{P}^i estimated at the stabilized waypoint's dynamic pressure q_0 with a perturbation to dynamic pressure δ_q^i , as in Fig. 3, define δ :

$$\delta = \min_{\delta_q^i > 0} \{\delta_q^i : F_l[\bar{P}^{(j)}, \delta_q^i] \text{ is unstable}\}, \quad (j = 2 \text{ or } 3)$$

Then the structured singular value $\mu(\bar{P}^{(j)})$ is computed as follows:

$$\mu(\bar{P}^{(j)}) = \frac{1}{\delta}$$

So

$$q_f = q_0 + \delta$$

is the nominal flutter pressure.

Hence, the flutter boundary, characterized by the flutter speed and frequency, is found by increasing the value of δ_q^i until an eigenvalue of the state matrix of $F_l[\bar{P}^{(j)}, \delta_q^i]$ has a positive real part, and the system becomes unstable.

Comparison Analysis: Zimmerman–Weissenburger Method (Flutter Margin)

For evaluation purposes, the Zimmerman–Weissenburger flutter margin (FM) is used [2]. Its basic concepts and analytical development are based on a two-degree-of-freedom analysis. The stability of the system is evaluated using Routh's criteria by requiring that all the coefficients of the characteristic equation need to be positive for a system to be stable.

For a binary system, the four roots of the characteristics equation are defined as follows:

$$\lambda_{1,2} = \beta_1 \pm j\omega_1 \quad \lambda_{3,4} = \beta_2 \pm j\omega_2$$

The FM is defined as follows [2]:

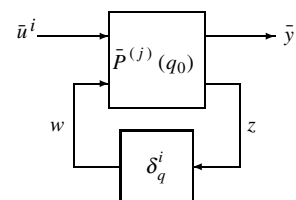


Fig. 3 Dynamic-pressure dependent PV model (with $j = 2$ or 3).

$$\begin{aligned} \text{FM} = & \left[\left(\frac{\omega_2^2 - \omega_1^2}{2} \right) + \left(\frac{\beta_2^2 - \beta_1^2}{2} \right) \right]^2 \\ & + 4\beta_1\beta_2 \left[\left(\frac{\omega_2^2 + \omega_1^2}{2} \right) + 2\left(\frac{\beta_2 + \beta_1}{2} \right)^2 \right] \\ & - \left[\left(\frac{\beta_2 - \beta_1}{\beta_2 + \beta_1} \right) \left(\frac{\omega_2^2 + \omega_1^2}{2} \right) + 2\left(\frac{\beta_2 + \beta_1}{2} \right)^2 \right]^2 \end{aligned} \quad (20)$$

Specifically, the FM corresponding to any airspeed will be evaluated using the already-estimated modal parameters of the aeroelastic system under analysis for both long-duration (frequency sweep) and short-duration (multistep, 3-2-1-1) excitation signals in the following two application cases. Therefore, it will be possible to predict how the FM will be at higher speeds by assuming a quadratic polynomial variation with the dynamic pressure q^i ; that is,

$$\text{FM} = f_{m0} + f_{m1}q^i + f_{m2}(q^i)^2 \quad (21)$$

The dynamic pressure associated with flutter is predicted by computing the FM from data taken at different waypoints, and then the roots of Eq. (21) provide the dynamic pressure at which flutter starts.

Application Cases

Two application cases were successfully solved using the algorithms developed throughout this work. These algorithms were proven to be robust enough to tolerate the low signal-to-noise ratio (SNR) inherent in flight-test data and to identify key parameters with limited data sets.

The first case study involved a generic pitch and plunge linear aeroelastic wind-tunnel model. This *easy-to-handle* dynamic system helps to validate the core algorithms upon which the framework is built. Either frequency sweeps or multistep 3-2-1-1 excitation signals (usually employed for flutter envelope-expansion and flying-quality evaluation programs) are used to accurately estimate the modal information embedded in the flight-test data. Three different flight-test environments were recreated by injecting additive noise at the output signal. These are the benign (SNR = 14 dB), moderate (SNR = 11 dB), and severe (SNR = 8.8 dB) flight-test-case environments.

Finally, flight-test data from the Aerostructure Test Wing (ATW) program were used to demonstrate the feasible application of the prototypical core algorithms using data coming from actual flight-test programs. In what follows, a brief summary is given of the results achieved using the short-duration 3-2-1-1 input under a severe test environment (SNR = 8.8 dB) for the first case study and for the second case using the actual flight-test data recorded at $H = 10$ kft and different Mach numbers.

Case I: Pitch–Plunge Aeroelastic System

To validate the PVE flutter-prediction framework, the pitch–plunge system's aeroelastic wind-tunnel model developed by the Department of Aerospace Engineering at Texas A&M University was selected. The geometry and main parameters to be used in the numerical simulations are those noted in Table 1. The model is composed of a rigid airfoil, the motion of which is restricted to pitching and plunging, mounted in a wind tunnel [15]. The dynamics of the system are described by Eq. (22):

$$\begin{aligned} & \begin{bmatrix} m_T & m_w x_\alpha b \\ m_w x_\alpha b & I_\alpha \end{bmatrix} \begin{bmatrix} \ddot{h} \\ \ddot{\alpha} \end{bmatrix} + \begin{bmatrix} c_h & 0 \\ 0 & c_\alpha \end{bmatrix} \begin{bmatrix} \dot{h} \\ \dot{\alpha} \end{bmatrix} + \begin{bmatrix} k_h & 0 \\ 0 & k_\alpha \end{bmatrix} \begin{bmatrix} h \\ \alpha \end{bmatrix} \\ & = 2\bar{q}b \begin{bmatrix} c_{l_\alpha} \left(\alpha + \frac{1}{U} \dot{h} + \left(\frac{1}{2} - a \right) b \frac{1}{U} \dot{\alpha} \right) + c_{l_\beta} \beta \\ c_{m_\alpha} \left(\alpha + \frac{1}{U} \dot{h} + \left(\frac{1}{2} - a \right) b \frac{1}{U} \dot{\alpha} \right) + c_{m_\beta} \beta \end{bmatrix} \end{aligned} \quad (22)$$

where the degrees of freedom of the rigid airfoil are described by the plunge h and the pitch α parameters. The left side of Eq. (22)

Table 1 Pitch-plunge system parameters

Geometric parameters	
Semichord b	0.135 m
Elastic axis e	-0.6
Mass parameters	
Mass m	12.387 kg
Inertial parameters	
x_α	0.2466
I_α	0.065 kg m ²
Damping parameters	
c_h	27.43 kg/s
c_α	0.180 kg m ² /s
Stiffness parameters	
k_h	2844.2 N/m
k_α	2.82 Nm/rad
k_{α^5}	70 Nm/rad
Aerodynamics parameters	
c_{l_α}	2π
c_{l_β}	3.358
c_{m_α}	-0.628
c_{m_β}	-0.635

describes the quasi-steady aerodynamic forces that are generated in response to the motion of the airfoil and commanded rotations β of a flap. The right side of the equality describes the structural dynamics behavior.

Input-Signal Generation

In system identification, the experiments carried out need to be informative enough; that is, the input signals need to be broadband and persistently exciting. Simply stated, the measured data should contain information of the system to be identified over a sufficiently wide frequency range. Hence, two different types of input signals were used to excite the aeroelastic pitch–plunge system. The first was a long-duration ($t \leq 32$ s) frequency-sweep sine signal, typically used in flutter envelope-expansion programs; the second was a short-duration ($t \leq 5$ s) multistep 3-2-1-1 input signal, usually designed for flying-quality testing purposes.

Figure 4 schematically shows the block diagram for the aeroelastic pitch–plunge system with the use of both long-duration sweep sine and short-duration multistep 3-2-1-1 input signals. The simulated measured system output is the pitch angle $\alpha(t)$, which is corrupted with a zero-mean Gaussian distributed white noise with a variable standard deviation σ , and the system input is the flap deflection $\beta(t)$.

It is well known that frequency sweeps have broadband characteristics and so the identified models usually present a good prediction capability [16]. However, they also can lead to relatively long maneuver times, and thus the aircraft has the tendency to depart from the intended trim flight condition. Based on these practical considerations, the multistep 3-2-1-1 input signal was designed in the 1970s [17] and mainly used for flying-quality purposes.

The 3-2-1-1 input is seven periods T long and consists of alternating positive and negative of equal magnitude with steps of relative durations 3, 2, 1, and 1 [18]. The physical characteristics of the 3-2-1-1 short-duration signal are shown in Fig. 5a, in which the period is defined as $T = 0.7/(2f_n)$, where f_n is the natural frequency (in hertz) of the dominant mode of the dynamical system. The energy spectrum is shown in Fig. 5b. From 5b it is observed that with the correct selection of the natural frequency f_n , the 3-2-1-1 input contains a wide frequency band of information that can also be used to excite the aeroelastic pitch–plunge system for flight flutter investigation purposes.

Modal Parameter Estimation

A zero-mean colored noise, with spectrum $\Phi_\epsilon = \sigma_i^2 / [1.2 - 0.4 \cos(\omega)]$, is embedded in the output data $\bar{y}_k = \alpha_k + \epsilon_k$. In this simple way, an approximate ramp-up approach is assumed for the noise component in the output signal to simulate poor-quality aeroelastic response data. The standard deviation σ_i is set to 40% of

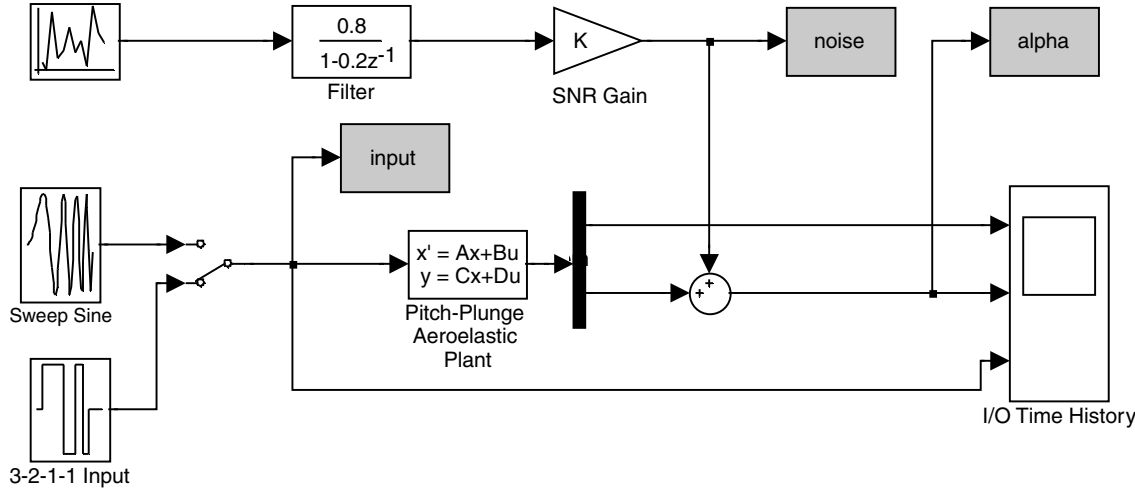
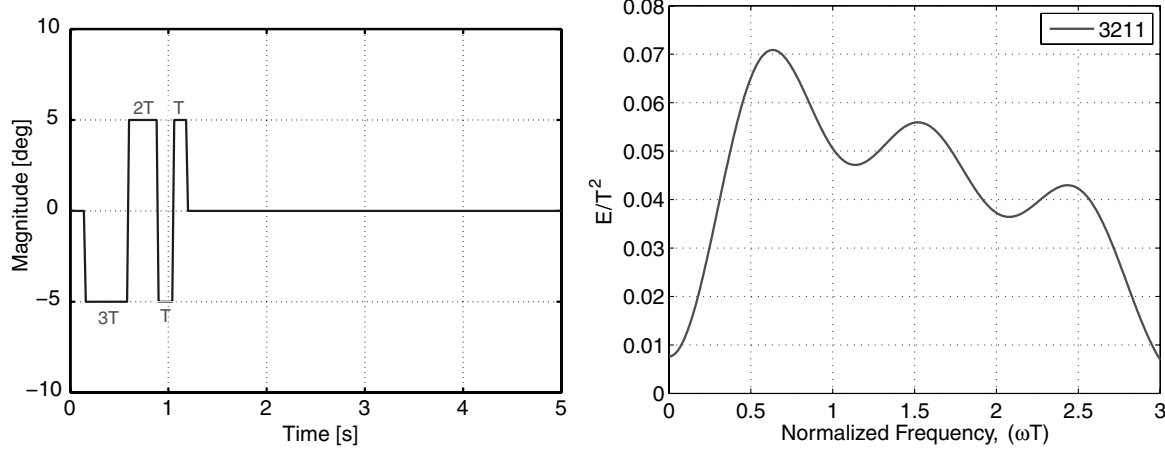


Fig. 4 Block diagram for the aeroelastic pitch–plunge system.



a) 3-2-1-1 Multistep input signal

b) Energy spectrum

Fig. 5 Short-duration 3-2-1-1 input signal.

the maximum absolute value of the maximum output \bar{y}_k for the noise-free ideal case ($\varepsilon_k = 0$). This test environment gives rise to a SNR value of 8.8 dB, mimicking the data recorded in actual flight-test programs. Responses are computed at airspeeds ranging from $U_0 = 3$ to 11 m/s, providing a set of 9 stable and safe test-point conditions. The FFT-based PolyMAX technique was used to estimate the physical modes from the input and output data. Estimation results with sweep sine signal excitation are shown in Table 2. Estimation results with 3-2-1-1 input excitation are shown in Table 3. Figure 6 shows the stabilization diagram at $U_0 = 10$ m/s with both sweep sine excitation and 3-2-1-1 excitation. From these clean diagrams it can be seen that the PolyMAX identification methodology is able to consistently estimate two physical modes.

It is observed from both tables that irrespective of the type of the excitation signal, the frequency content of the modes embedded are consistently estimated. However, the damping-ratio value estimation is biased in this testing environment (SNR = 8.8 dB). Regarding the biased damping-ratio estimation, it is known that frequency-response-based methods work better for highly damped systems that exhibit broad resonance peaks in the frequency domain than for lightly damped systems. This is mainly due to the fact that in the highly damped systems, the peaks are spread over several spectral lines. Nevertheless, it will be shown in the ensuing sections that the selected identification approach is able to recover the key modal dynamic characteristics embedded in the simulated flight-test data even though the modal damping-ratio estimation is biased.

Linear Operator Identification

Responses of the pitch–plunge system are simulated using the model shown in Fig. 4 at waypoint airspeed values ranging from $U_0 = 3$ to 11 m/s. Hence, a total of 9 responses at stable and safe waypoints are generated for the testing environment of SNR = 8.8 dB. It is assumed that the experimental data $\{y_k^{i-}, u_k^{i-}\}_{k=1}^{N_p}$ ($i = U_0 \in [3, \dots, 11]$ m/s) can be explained by the following linear operator:

$$\bar{P}_i = \sum_{l=0}^{p-1} b_l B_l(q), \quad i = U_0 \in [3, \dots, 11] \quad (23)$$

The required modal parameters needed to tune the set of basis functions $\{B_l(q)\}_{l=0}^{p-1}$ are, namely, the set composed of the natural frequencies ω_k and damping ratios ζ_k (i.e., $\{\omega_k, \zeta_k\}_{k=1}^{N_p}$, where N_p is the number of single modes estimated from the data). Hence, using the modal data noted in Tables 2 and 3, the related \bar{P}_i systems are estimated at each waypoint with velocity $i = U_0$.

The pitch angle in response to the sweep sine command is shown in Fig. 7 for a selected subset of airspeed values (i.e., $U_0 = [4, 6, 8, 10]$ m/s). Figures 7a–7d show (solid line) the measured (simulated) pitch response $\bar{y}_k^i = \alpha_k + \varepsilon_k$, together with the response achieved from the identified linear operator $\bar{y}_k^i = \bar{P}_i \bar{u}_k^i$ (dotted line).

In addition, Fig. 7e shows the unmodeled dynamics, $e_k = \bar{y}_k^i - y_k$, between the measured pitch angle and its estimated counterparts

Table 2 Estimated modes using the FFT-based Polymax method with sweep sine signal excitation (SNR 8.8 dB)

Airspeed U_0 , m/s	Mode no.	Physical modes		PolyMAX identification	
		Frequency, Hz	Damping, δ , %	Frequency, Hz	Damping, δ , %
3	1	1.06	20.48	1.06	17.87
	2	2.74	20.74	2.72	1.10
4	1	1.09	20.62	1.09	17.99
	2	2.72	10.68	2.69	1.88
5	1	1.12	20.72	1.13	17.98
	2	2.69	10.60	2.66	2.63
6	1	1.17	20.81	1.18	17.78
	2	2.65	10.60	2.63	3.20
7	1	1.22	20.91	1.24	17.59
	2	2.60	10.33	2.57	3.89
8	1	1.28	21.07	1.31	16.96
	2	2.54	10.07	2.50	3.87
9	1	1.37	21.39	1.40	16.17
	2	2.47	9.62	2.42	4.45
10	1	1.47	22.10	1.51	15.27
	2	2.37	8.77	2.33	4.76
11	1	1.61	24.00	1.61	13.72
	2	2.24	6.70	2.25	3.96

Table 3 Estimated modes using FFT-based Polymax method with 3-2-1-1 signal excitation (SNR = 8.8 dB)

Airspeed U_0 , m/s	Mode no.	Physical modes		PolyMAX identification	
		Frequency, Hz	Damping, δ , %	Frequency, Hz	Damping, δ , %
3	1	1.06	20.48	0.99	23.32
	2	2.74	20.73	2.66	0.82
4	1	1.08	20.62	1.02	23.81
	2	2.72	10.68	2.66	1.28
5	1	1.12	20.72	1.06	23.79
	2	2.68	10.60	2.66	2.13
6	1	1.16	20.81	1.12	23.29
	2	2.65	10.60	2.65	3.06
7	1	1.22	20.90	1.18	23.14
	2	2.60	10.33	2.63	3.81
8	1	1.28	21.07	1.25	24.26
	2	2.54	10.07	2.59	3.30
9	1	1.37	21.39	1.36	24.41
	2	2.46	9.62	2.53	2.78
10	1	1.47	22.10	1.52	22.68
	2	2.37	8.77	2.38	2.11
11	1	1.61	24.00	1.76	22.18
	2	2.24	6.70	2.28	4.49

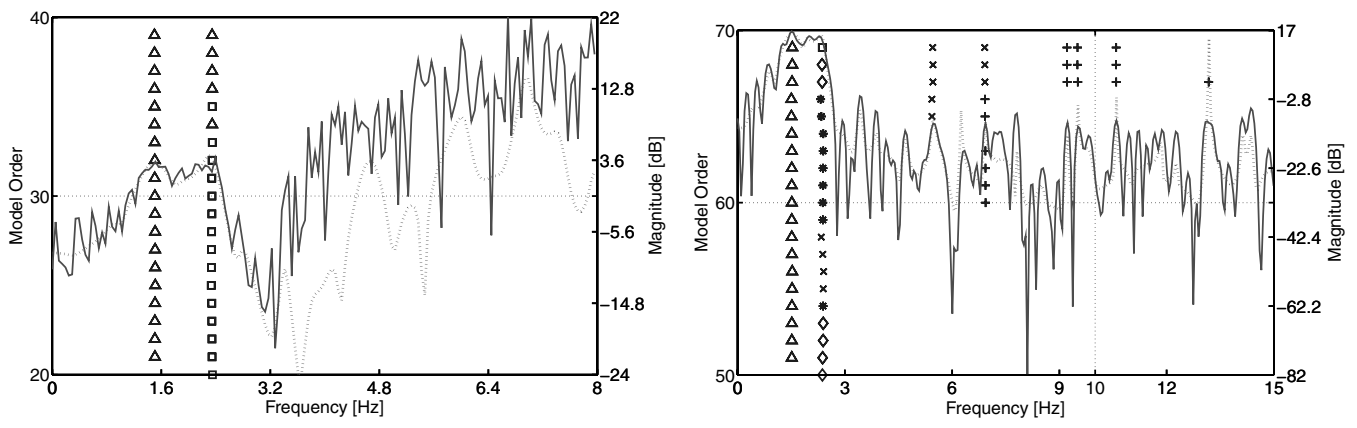
**a) Sweep sine input****b) 3-2-1-1 Input**

Fig. 6 Stabilization diagram of the aeroelastic system at $U_0 = 10$ m/s with parameter constraint $A_{ua} = 1$ and SNR = 8.8 dB; spectral estimate of the physical system (solid line) and approximation with the 40th-order model (dotted line).

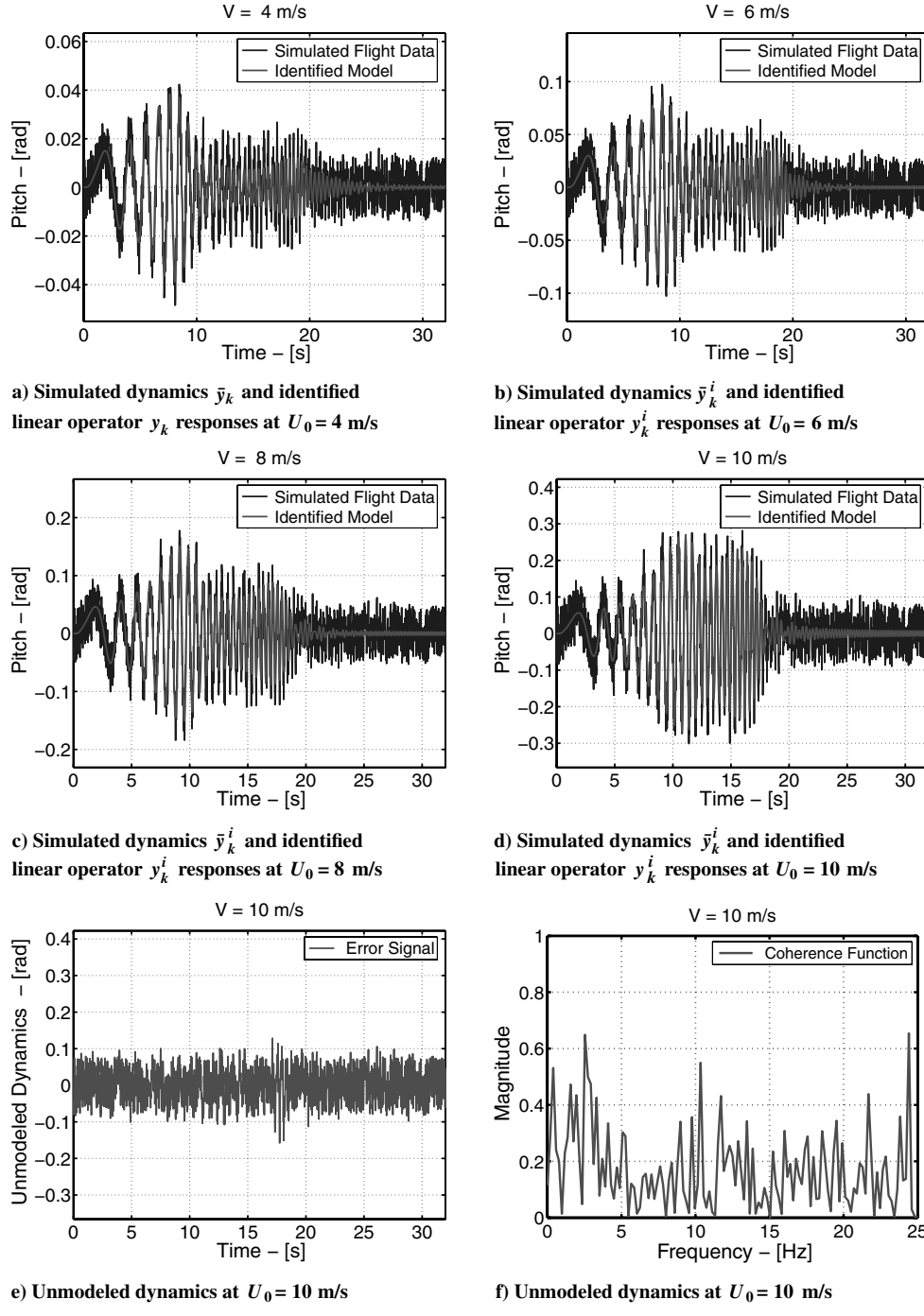


Fig. 7 Simulated and identified pitch angle response to a sweep sine input at SNR = 8.8 dB.

coming from the linear dynamics operator \bar{P}_{10} . The unmodeled dynamics can be used to inspect the accuracy of the estimated system dynamics by calculating the correlation between the input signal \bar{u}_k^i and unmodeled dynamics e_k . Figure 7f shows the related correlation function for the waypoint airspeed $U_0 = 10 \text{ m/s}$. Coherence is a function of frequency with values between 0 and 1 that indicates how well the input X corresponds to the output Y at each frequency. Hence, if the correlation function is smaller than 1, then the input and unmodeled dynamics are not correlated, and the estimated model already includes the essential dynamics contained in the input/output data set.

Similarly, the pitch angle responses to the short-duration multistep 3-2-1-1 input signal are shown in Fig. 8 for the same testing environment conditions: $U_0 = [4, 6, 8, 10] \text{ m/s}$ and SNR = 8.8 dB. It is observed that a very good agreement is achieved between the measured and identified responses.

From this set of figures it can be concluded that the proposed framework composed of the FFT-based PolyMAX plus the system-identification techniques is able to accurately represent the experimental data collected at each stabilized waypoint using long-duration ($t \leq 32 \text{ s}$) and short-duration ($t \leq 5 \text{ s}$) input signals, even though the modal damping-ratio estimation was not accurately performed. In addition, these algorithms are robust enough to tolerate the low SNR quantity used throughout this case study.

Flutter-Boundary Prediction

At each dynamic pressure, a parameter-varying model is computed based on a least-squares fit of the identified models. The models at each stabilized waypoint of increasing dynamic pressures are computed by accounting for the data measured at that dynamic pressure, blended with data from the previous waypoints.

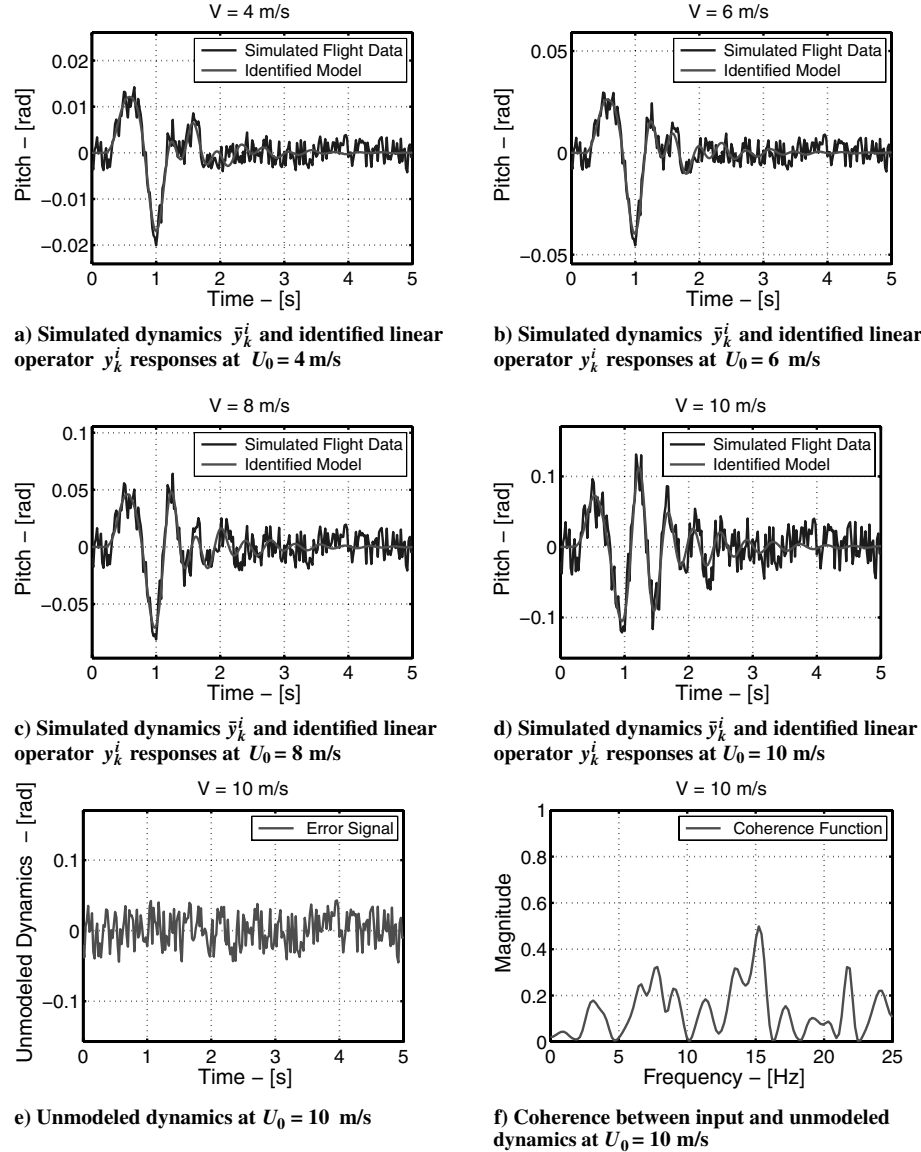


Fig. 8 Simulated and identified pitch angle response to a 3-2-1-1 input at SNR = 8.8 dB.

For evaluation purposes the FM method is used [2]. Its basic concepts and analytical development are based on a two-degree-of-freedom analysis. The stability of the system is evaluated using the Routh's criteria by requiring that all the coefficients of the characteristic equation be positive for a system to be stable.

The airspeed and frequency at which flutter is predicted to occur with both long-duration sweep sine input and short-duration 3-2-1-1 input are shown in Tables 4 and 5, using both the FM method and the PVE (quadratic and cubic matrix polynomial functions) techniques, respectively. Note that both flutter-prediction techniques use the

same modal parameter information estimated by the FFT-based PolyMAX method. N/A in Table 5 means that out-of-range values were predicted by the FM method at that particular waypoint's airspeed.

In each one of these tables, the first column indicates the model designation; that is, the actual model (true) or the parameter-varying model $F_l[\bar{P}^{(2)}, \delta_q^i]$. The second column indicates the flutter speed predicted using the FM technique, and the last two columns are related with the proposed PVE framework. The aeroelastic pitch-plunge model under analysis, the so-called true model, reached its

Table 4 Predicted flutter-boundary summary with sweep sine input (SNR = 8.8 dB)

Waypoint	FM	PVE(q^2)	PVE(q^3)
Aeroelastic plant	Flutter speed, m/s	Flutter speed, m/s	Flutter speed, m/s
True	12.11	12.11	12.11
$F_l[\bar{P}_5^{(2)}, \delta_q^i]$	8.11	8.88	7.37
$F_l[\bar{P}_6^{(2)}, \delta_q^i]$	8.48	9.39	9.39
$F_l[\bar{P}_7^{(2)}, \delta_q^i]$	9.98	9.99	9.99
$F_l[\bar{P}_8^{(2)}, \delta_q^i]$	10.24	10.63	10.63
$F_l[\bar{P}_9^{(2)}, \delta_q^i]$	11.26	11.33	11.33
$F_l[\bar{P}_{10}^{(2)}, \delta_q^i]$	11.52	12.07	12.07
$F_l[\bar{P}_{11}^{(2)}, \delta_q^i]$	11.72	12.00	12.09

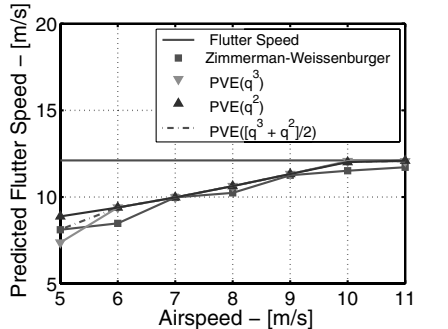
Table 5 Predicted flutter-boundary summary with 3-2-1-1 input (SNR = 8.8 dB)

Waypoint	FM	PVE(q^2)	PVE(q^3)
Aeroelastic plant	Flutter speed, m/s	Flutter speed, m/s	Flutter speed, m/s
True	12.11	12.11	12.11
$F_l[\bar{P}_5^{(2)}, \delta_q^1]$	N/A	8.88	8.88
$F_l[\bar{P}_6^{(2)}, \delta_q^1]$	N/A	9.39	7.75
$F_l[\bar{P}_7^{(2)}, \delta_q^1]$	13.15	9.99	9.99
$F_l[\bar{P}_8^{(2)}, \delta_q^1]$	10.63	10.63	10.63
$F_l[\bar{P}_9^{(2)}, \delta_q^1]$	10.27	11.33	11.33
$F_l[\bar{P}_{10}^{(2)}, \delta_q^1]$	10.55	12.07	12.07
$F_l[\bar{P}_{11}^{(2)}, \delta_q^1]$	11.52	12.09	12.09

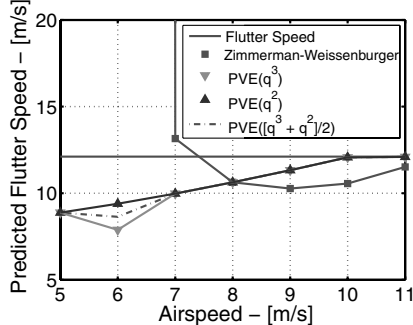
instability boundary $V_{f_{\text{true}}} = 12.11$ m/s with an oscillatory frequency of $\omega_{f_{\text{true}}} = 2.11$ Hz.

Figure 9a summarizes Table 4, and Fig. 9b summarizes Table 5. In both figures, the horizontal axis represents the stabilized waypoint's airspeed, the vertical axis indicates the predicted flutter speed by each method, and the horizontal solid line indicates the flutter boundary. Note that in addition to the FM and the quadratic PVE [PVE(q^2)] methods, the cubic matrix polynomial function [PVE(q^3)] as well as an average value are also included in the plot. It is observed that even using the same modal information for both methods, the PVE framework always provides a more accurate flutter-boundary prediction than the traditional FM approach.

Specifically, using both long-duration and short-duration signals, the PVE framework achieves, under a testing environment mimicking real flutter flight-test conditions, a flutter speed of $\bar{V}_f = 12.09$ m/s and a frequency estimation varying between $\bar{\omega}_f = 2.11$ Hz and $\bar{\omega}_f = 2.14$ Hz (see Tables 4 and 5). These values are practically the same as the actual values of $V_{f_{\text{true}}}$ and $\omega_{f_{\text{true}}}$. In addition, it can be observed that the PVE framework provides a consistent flutter-instability boundary estimation from the waypoint's airspeed $U_0 = 10$ m/s. All of these features clearly outperform the FM results of [2].



a) Flutter prediction at SNR = 8.8 dB with sweep sine input signal



b) Flutter prediction at SNR = 8.8 dB with multistep 3-2-1-1 input signal

Fig. 9 Flutter predictor using long-duration sweep sine input and multistep 3-2-1-1 input.

Case II: Aerostructure Test Wing Flight Test at $H = 10$ kft

This case study is included to demonstrate the feasible application of the core PVE algorithms to data coming from actual flutter flight-envelope programs. The ATW structure developed at NASA Dryden Flight Research Center was a realistic structure similar to an aircraft wing [19]. The ATW was flown on the F-15B flight-test fixture. The wing was built based on a NACA-65A004 airfoil shape. The wing had a half-span of 18 in. with a root chord length of 13.2 in. and tip chord 8.7 in. The total weight is 1.66 lb. The description of the ATW is shown in Table 6. The assembly is shown in Fig. 10, in which Fig. 10a is the ATW structure, and Fig. 10b illustrates how the ATW structure was mounted horizontally to the F-15 fuselage fixture.

ATW Model: Physical Frequency and Damping Estimation

During the flight-test program, sinusoidal frequency sweeps between 5 to 35 Hz were used as the input signal to excite the ATW structure. The flight-test program followed standard procedures for envelope expansion. The ATW was flown during four flight tests that included 21 test points at Mach numbers between $M = 0.5$ and 0.82 and altitudes between $H = 10$ and 20 kft. Here, only the flight-test data obtained from height $H = 10$ kft are considered to estimate the physical modes of the ATW system.

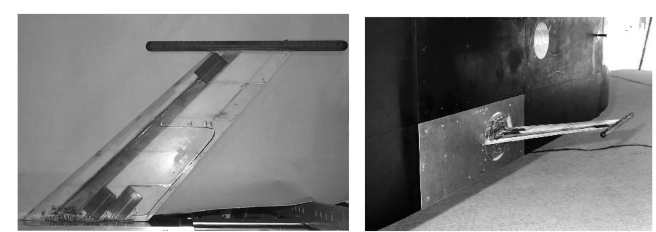
As in the previous test cases, the FFT-based PolyMAX method is applied to estimate the modal parameters (i.e., natural frequency and damping) contained in the data. The stabilization diagrams for several Mach numbers, varying between $0.7 \leq M \leq 0.82$, at $H = 10$ kft are shown in Fig. 11, and it is observed that two physical modes can be consistently estimated. The estimation results for the physical frequencies and dampings of the ATW system at $H = 10$ kft are summarized in Table 7.

ATW Structure: Linear Operator Identification

A set of orthonormal basis functions $\{B_l(q)\}_{l=0}^3$ are generated based on the estimated frequency and damping of the ATW system noted in Table 7. These orthonormal basis functions constitute the a priori information needed for the block-oriented system-identification approach to accurately estimate the ATW dynamics. Hence, it is assumed that the experimental data $\{\tilde{y}_k^i, \tilde{u}_k^i\}_{k=1}^N$, where

$$i = U_0 \in [274, 301, 330, 356, 383, 411, 437, 450] \text{ KEAS}$$

and k is the k th experimental sample, can be explained by the linear operator \tilde{P}_i :



a) ATW structure b) Mounting of the ATW

Fig. 10 ATW system.

Table 6 ATW wing structure description

Half-span	18 in.	Root chord	13.2 in.
Tip chord	8.7 in.	Semispans area	197 in. ²
Aspect ratio	3.28	Airfoil	NACA65A004
Taper ratio	0.659	Sweepback quarter chord	45 deg
Mass material	Powered tungsten carbide	Sensors	Accel. and strain gauges
Nonstructural mass	0.66 lb	Total wing weight	1.66 lb

$$\bar{P}_i = \sum_{l=0}^3 b_l B_l(q), \quad i = U_0 \quad (24)$$

The estimation results can now be evaluated by comparing the flight's measured acceleration response with the simulated model response, as well as using the correlations between the input signal \bar{u}_k^i and error dynamics $e_k^i = \bar{y}_k^i - y_k^i$.

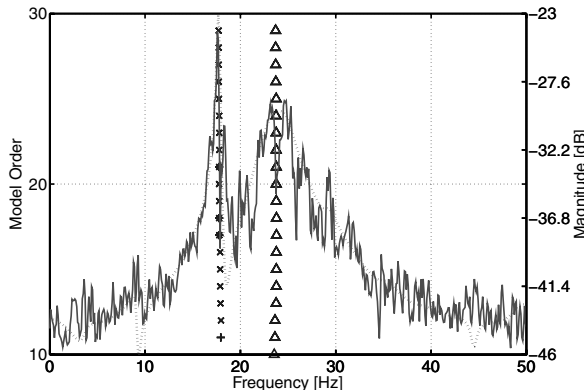
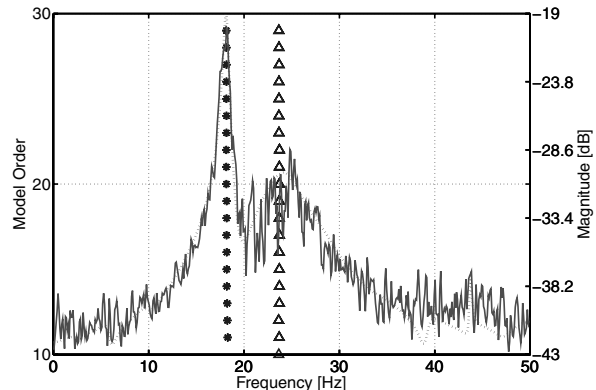
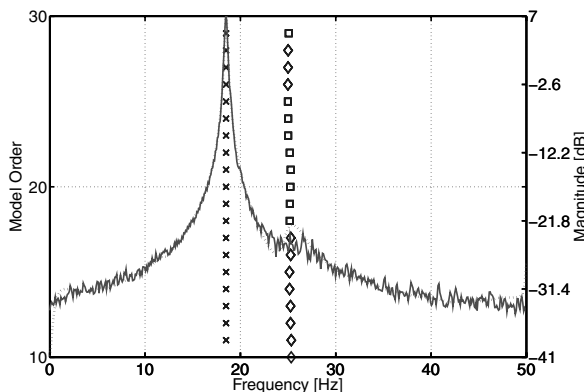
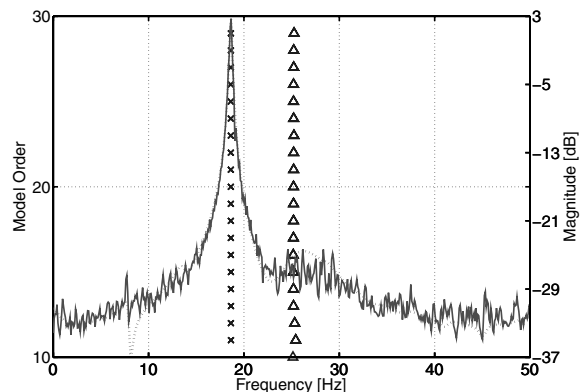
As an example, Fig. 12 shows the model-estimation results for two waypoints, $V_{\text{way}} = 356$ KEAS ($M = 0.65$ and $H = 10$ kft) and $V_{\text{way}} = 437$ KEAS ($M = 0.80$ and $H = 10$ kft), considered at $H = 10$ kft. The SNR testing scenarios are actually very low, ranging approximately between $\text{SNR} = 0.9$ and 4 dB. From Fig. 12 it is observed that the main modal components present at the ATW's acceleration signals are consistently estimated at both waypoints.

The novel PVE framework and the FM method [2] are used to predict the ATW flutter onset using a varying-Mach envelope-expansion approach. Table 8 shows the airspeed and frequency at which flutter is predicted to occur using both techniques.

Figure 13 summarizes Table 8. The horizontal axis represents the stabilized waypoint's airspeed, the vertical axis indicates the predicted flutter speed by each method, and the horizontal solid line indicates the flight-recorded flutter speed boundary. In addition to the flutter margin and the quadratic PVE(q^2) methods, the cubic matrix

Table 7 Estimated modes using FFT-based PolyMAX method at height 10 kft

Mach, height	Airspeed, KEAS	PolyMAX identification	
		Frequency, Hz	Damping δ , %
0.5, 10 kft	274	15.77	9.38
		22.43	4.94
0.55, 10 kft	301	16.30	6.76
		22.93	4.97
0.60, 10 kft	330	16.87	5.93
		23.40	5.71
0.65, 10 kft	356	17.19	4.01
		23.75	6.89
0.70, 10 kft	383	17.58	4.30
		23.87	7.74
0.75, 10 kft	411	17.93	2.97
		24.52	9.89
0.80, 10 kft	437	18.51	0.77
		24.53	12.26
0.82, 10 kft	450	18.58	0.81
		24.10	9.17

a) Stabilization diagram at $M = 0.7$ and $H = 10$ Kftb) Stabilization diagram at $M = 0.75$ and $H = 10$ Kftc) Stabilization diagram at $M = 0.8$ and $H = 10$ Kftd) Stabilization diagram at $M = 0.82$ and $H = 10$ Kft**Fig. 11** Stabilization diagrams for the ATW system at $H = 10$ kft and different Mach numbers.

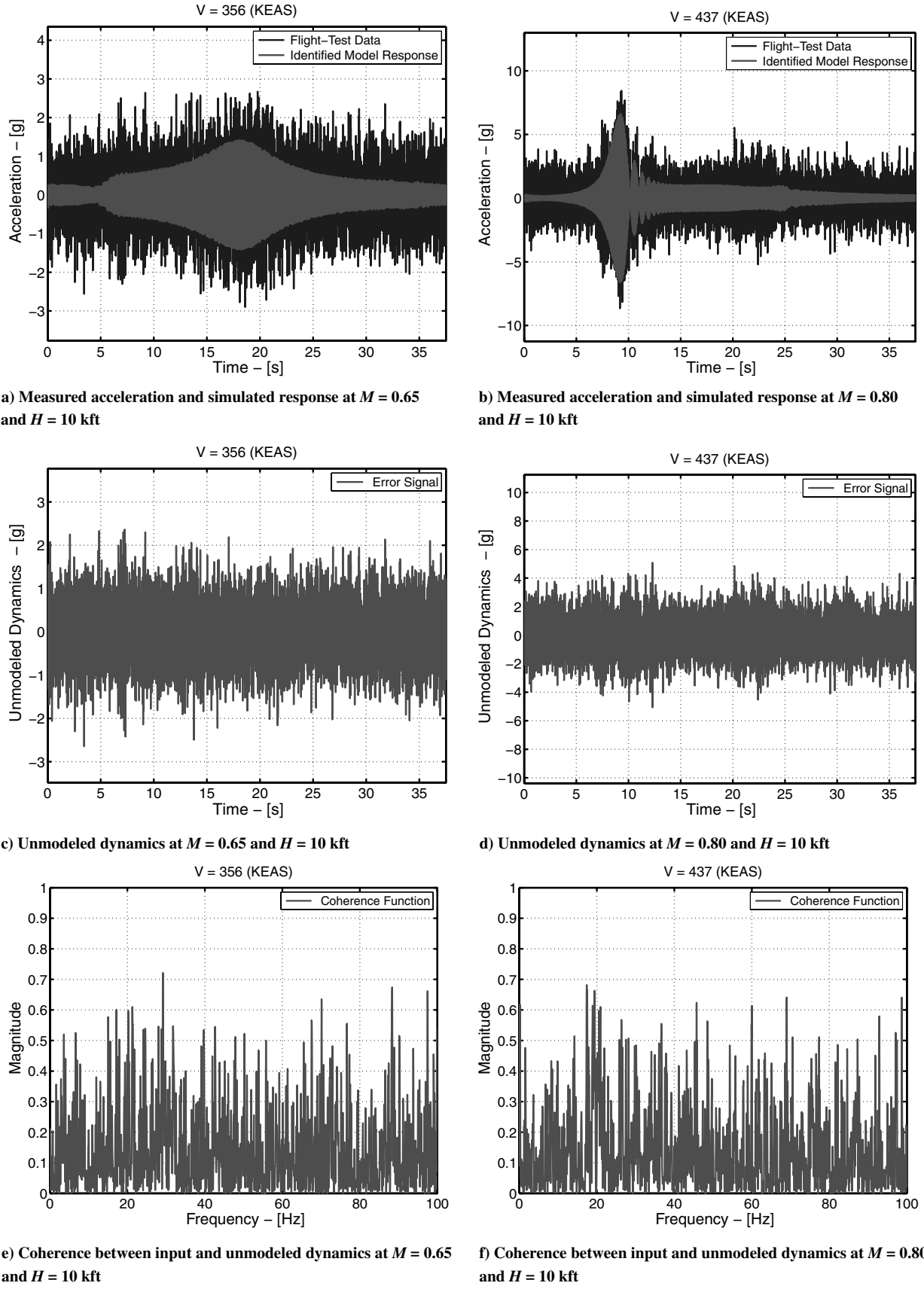


Fig. 12 Measured and identified acceleration responses.

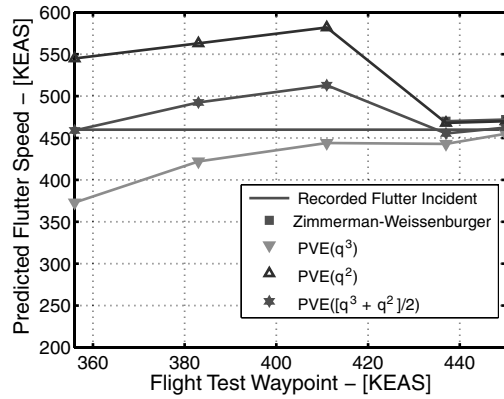
polynomial function $\text{PVE}(q^3)$ as well as the average-value $\text{PVE}([q^2 + q^3]/2)$ are also included in this figure.

It is observed that the FM method is unable to provide a valid estimation of the flutter speed from the first three waypoints

($V_{\text{way}} = 356, 383$, and 411 KEAS). These points are labeled as N/A (not available) for prediction. For the last higher-speed waypoints, the FM approach slightly overpredicts the actual flutter-instability boundary (red).

Table 8 ATW flight-test program at $H = 10$ kft predicted flutter boundary

Waypoint	FM	PVE(q^2)		PVE(q^3)		PVE (avg)	
		Airspeed, KEAS	Flight speed, KEAS	Flight speed, KEAS	Flight frequency, Hz	Flight speed, KEAS	Flight frequency, Hz
Recorded		460	460	460	19.30	460	19.30
356	N/A	543	543	373	13.29	459	16.26
383	N/A	563	563	422	15.40	492	21.54
411	N/A	582	582	444	16.54	513	16.60
437	470	468	468	443	19.40	456	19.19
450	4.72	470	470	455	19.40	462	19.41

**Fig. 13** Predicted flutter speed during varying-Mach envelope expansion at $H = 10$ kft.

Both $\text{PVE}(q^2)$ and $\text{PVE}(q^3)$ are able to provide a flutter airspeed estimation at each of the waypoints, the former being an optimistic prediction by overpassing the flutter boundary when using data from low-speed waypoints of less than 437 KEAS ($M = 0.8$ and $H = 10$ kft). Similar to the FM approach, the $\text{PVE}(q^2)$ is able to provide a fair flutter-boundary estimation using data that includes the high-speed waypoints of $V_f = 437$ and 450 KEAS ($M = 0.8$ and 0.82, $H = 10$ kft).

Conversely, the $\text{PVE}(q^3)$ just from the initial waypoint provides a realistic prediction for the two main flutter parameters (that is, the flutter speed and frequency), never exceeding the recorded flutter-instability boundary as the envelope is expanded to include higher-speed waypoints. In addition, it is worth mentioning that the PVE 's average-value $\text{PVE}([q^2 + q^3]/2)$ is also able to predict the flutter-instability value right at the initial waypoint of $V_f = 356$ KEAS ($M = 0.5$ and $H = 10$ kft), and then the prediction is close to the actual flutter boundary from the last two waypoints of $V_f = 437$ and 450 KEAS ($M = 0.8$ and 0.82 and $H = 10$ kft).

Thus, a preliminary criterion based on these two case studies is to observe how the predicted flutter boundary using both $\text{PVE}(q^2)$ and $\text{PVE}(q^3)$ evolves as the waypoint dynamic pressure is varied. If the $\text{PVE}(q^2)$ flutter-prediction value is close enough to the $\text{PVE}(q^3)$ predicted value, then the aircraft is presumably reaching its flutter-instability point and the test needs to be terminated.

Conclusions

In this paper, we introduced an alternative strategy to predict the flutter onset that tolerates real-world flight-testing environments during aircraft or store separation envelope-expansion programs. The formulation of a novel parameter-varying flutter-prediction capability using data-based aeroelastic parameter-varying operators defined at each stable waypoint has been presented. In particular, a method was shown to obtain a general framework to represent parameter estimation with flight-condition dependency.

Either frequency sweeps or multistep 3-2-1-1 excitation signals were used to accurately estimated the modal information embedded in the characteristic low-signal-to-noise-ratio flight-test data. Even though the latter represent short-duration maneuvers, typically used

in flying-quality certification programs, the aeroelastic parameter-varying models accurately estimated the flutter onset using these limited data sets.

Simulated and actual flight-test data were used to successfully illustrate the parameter-varying flutter-prediction tool capabilities. Based on the presented results, it is found that the proposed blended aeroelastic parameter-varying model generation and flutter-prediction approach provides an enabling and dependable tool. Its use will presumably reduce the cost and time required to clear the aircraft envelope; therefore, a more efficient aircraft certification process is expected to be performed.

Acknowledgment

Research supported by Edwards Air Force Base under Small Business Innovative Research Phase I contract FA9302-06-M-0004. This material has no affiliation with Northrop Grumman Corporation.

References

- [1] Kehoe, M. W., "A Historical Overview of Flight Flutter Testing," *NASA TM-4720*, Oct. 1995.
- [2] Zimmerman, N. H., and Weissenburger, J. T., "Prediction of Flutter Onset Speed Based on Flight Testing at Subcritical Speeds," *Journal of Aircraft*, Vol. 1, No. 4, 1964, pp. 190–202.
doi:10.2514/3.43581
- [3] Pototzky, A. S., Wieseman, A. S., Hoadley, C. D., and Mukhopadhyay, V., "On-Line Performance Evaluation of Multi-Loop Digital Control Systems," *Journal of Guidance, Control, and Dynamics*, Vol. 15, No. 4, July–Aug. 1992, pp. 878–884.
doi:10.2514/3.20920
- [4] Bukan, J. J., "Flight-Determined Multivariable Stability Analysis and Comparison of a Control System," *Journal of Guidance, Control, and Dynamics*, Vol. 16, No. 6, 1993, pp. 1026–1031.
doi:10.2514/3.21123
- [5] Lind, R., "Flight-Test Evaluation of Flutter Prediction Methods," *Journal of Aircraft*, Vol. 40, No. 5, 2003, pp. 964–970.
doi:10.2514/2.6881
- [6] Lind, R., Brenner, M., and Freudinger, L., "Improved Flight Test Procedures for Flutter Clearance," *International Forum on Aeroelasticity and Structural Dynamics*, Univ. of Rome "La Sapienza," Rome, June 1997, pp. 79–86.
- [7] Lind, R., Prazenica, R. J., Brenner, M. J., and Baldelli, D. H., "Identifying Parameter-Dependent Volterra Kernels to Predict Aeroelastic Instabilities," *AIAA Journal*, Vol. 43, No. 12, Nov.–Dec. 2005, pp. 2496–2502.
doi:10.2514/1.12042
- [8] Baldelli, D. H., Lind, R., and Brenner, M., "Nonlinear Aeroelastic/Aeroservoelastic Modeling Update by Block-Oriented Identification," *Journal of Guidance, Control, and Dynamics*, Vol. 28, No. 5, Sept.–Oct. 2005, pp. 1056–1064.
doi:10.2514/1.11792
- [9] Boukarim, G. E., and Chow, J. H., "Modeling of Nonlinear System Uncertainties Using a Linear Fractional Transformation Approach," *Proceedings of the American Control Conference*, Inst. of Electrical and Electronics Engineers, Piscataway, NJ, June 1998, pp. 2973–2979.
- [10] Lind, R., "Match-Point Solutions for Robust Flutter Analysis," *Journal of Aircraft*, Vol. 39, No. 1, Jan.–Feb. 2002, pp. 91–99.
doi:10.2514/2.2900
- [11] Cauberghe, B., Guillaume, P., Verboven, P., Parloo, E., and Vanlanduit, S., "A Poly-Reference Implementation of the Maximum

- Likelihood Complex Frequency-Domain Estimator and some Industrial Applications," *22nd International Modal Analysis Conference*, Inst. of Electrical and Electronics Engineers, Piscataway, NJ, Jan. 2004.
- [12] Cauberghe, B., Guillaume, P., Verboven, P., Vanlanduit, S., and Parloo, E., "On the Influence of the Parameter Constraint on the Stability of the Poles and the Discrimination Capabilities of the Stabilization Diagrams," *Mechanical Systems and Signal Processing*, Vol. 19, No. 5, 2005, pp. 989–1014.
doi:10.1016/j.ymssp.2004.07.007
- [13] Wahlberg, B., and Olivera e Silva, T., *Modelling and Identification with Rational Orthogonal Basis Functions*, Springer–Verlag, London, 2005, pp. 15–39.
- [14] Lind, R., and Brenner, M., *Robust Aeroseervoelastic Stability Analysis: Flight Test Applications*, Springer–Verlag, London, 1999.
- [15] Ko, J., Kurdila, A. J., and Strganac, T. W., "Nonlinear Control of a Prototypical Wing Section with Torsional Nonlinearity," *Journal of Guidance, Control, and Dynamics*, Vol. 20, No. 6, 1997, pp. 1181–1189.
doi:10.2514/2.4174
- [16] Klein, V., and Morelli, E. A., *Aircraft System Identification: Theory and Practice*, AIAA Education Series, AIAA, Reston, VA, 2006.
- [17] Plaetschke, E., Mulder, J. A., and Breeman, J. H., "Flight Test Results of Five Input Signals for Aircraft Parameter Identification," *Proceedings of the Sixth IFAC Symposium on Identification and System Parameter Estimation*, Inst. of Electrical and Electronics Engineers, Piscataway, NJ, 1982, pp. 1149–1154.
- [18] Jategaonkar, R. V., *Flight Vehicle System Identification: A Time Domain Methodology*, Progress in Astronautics and Aeronautics, AIAA, Reston, VA, 2006.
- [19] Lind, R., Voracek, D., Truax, R., Doyle, T., Potter, S., and Brenner, M., "A Flight Test to Demonstrate Flutter and Evaluate the Flutterometer," *The Aeronautical Journal*, Vol. 107, No. 1076, Oct. 2003, pp. 577–588.